Dalton Transactions

MX-type single chain complexes with aromatic in-plane ligand: incorporation of aromatic interactions for stabilizing chain structure

Journal:	*Dalton Transactions*
Manuscript ID	DT-ART-02-2019-000784.R1
Article Type:	Paper
Date Submitted by the Author:	19-Apr-2019
Complete List of Authors:	Afrin, Unjila; Tohoku University, Department of Chemistry, Graduate School of Science Iguchi, Hiroaki; Tohoku University, Department of Chemistry, Graduate School of Science Mian, Mohammad; Tohoku University, Department of Chemistry, Graduate School of Science Takaishi, Shinya; Tohoku University, Chemistry Yamakawa, Hiromichi; The university of Tokyo, Applied Physics Terashige, Tsubasa; AIST-UTokyo Advanced Operando-Measurement Technology Open Innovation Laboratory Miyamoto, Tatsuya; The university of Tokyo, Applied Physics Okamoto, Hiroshi; The university of Tokyo, Applied Physics Yamashita, Masahiro; Tohoku University, Department of Chemistry, Graduate School of Science

Journal Name

ARTICLE

MX-type single chain complexes with aromatic in-plane ligand: incorporation of aromatic interactions for stabilizing chain structure

Received 00th January 20xx,
Accepted 00th January 20xx

DOI: 10.1039/x0xx00000x

www.rsc.org/

Unjila Afrin,[a] Hiroaki Iguchi,*[,a] Mohammad Rasel Mian,[a] Shinya Takaishi,[a] Hiromichi Yamakawa,[b] Tsubasa Terashige,[c] Tatsuya Miyamoto,[b] Hiroshi Okamoto,[b,c] and Masahiro Yamashita*[,a,d,e]

MX-type one-dimensional complexes $[Pt^{IV}(amp)_2Br_2][Pt^{II/IV}(amp)_2Br]_2(HSO_4)_2(SO_4)_2\cdot 13H_2O$ (**3**) and $[Pt^{IV}(amp)_2Br_2][Pt^{II/IV}(amp)_2Br]_2(H_2PO_4)_6\cdot 8H_2O$ (**4**) were synthesized as the first analogue containing only aromatic in-plane ligand. The Pt–Br chain structures of **3** and **4** are stabilized by both hydrogen-bond network along the chain and the π-stacking via intercalated Pt(IV) complexes. Structural and spectroscopic studies indicated that both **3** and **4** form Pt(II/IV) mixed valence state.

Introduction

Organic-inorganic hybrid materials with one-dimensional (1D) electron system[1] such as "Quasi-1D halogen-bridged metal complexes" (so-called MX chains) have attracted much attention, because they have unique intrinsic physical properties. So far, mid-gap absorptions attributable to solitons and polarons,[2] gigantic third-order nonlinearities,[3] ultrafast optical responses,[4] spin-Peierls transition[5] etc. have been discovered in MX chains. The advantages of MX chains over other 1D materials such as carbon nanotubes and semiconducting inorganic nanowires are the controllability of their electronic states by changing their components (metal ions, bridging halides, in-plane ligands, and counteranions). For instance in PdBr chains, uncommon Pd(III) averaged valence (AV) state was achieved by introducing hydroxy group to the in-plane ligand[6] or long alkyl chains in the counteranions.[7] The introduction of π-conjugated ligand to MX chains is another methodology to modify the structure and electronic properties of MX chains. Moreover, the ease of synthetic modifications of π-conjugated system compared with aliphatic ligands should increase the diversity of MX chains. However, only a few aromatic ligands have been introduced in MX chains. For instance, 4,4'-bipyridine (bpy) connects two adjacent single-type MX chains to form ladder-[8] and tube-type[9] MX chains. These complexes, however, also contain aliphatic in-plane ligands such as ethylenediamine (en) and diethylenetriamine (dien), which provide hydrogen-bond network indispensable for stabilizing chain structure. Hence, to the best of our knowledge, aromatic ligands have not been used alone as in-plane ligands of single-type MX chains.

Since the chain structure is supported by the hydrogen bonds between counteranions and the amino group of in-plane ligands, at least half of the equatorial coordination position should be covered by amino group. In addition, aromatic amines are not favourable because they are less flexible and is oxidized in the synthetic condition of MX chains. Therefore, the chelate ligand consisting of both aromatic moiety and aliphatic amino group is required. In this work, we chose 2-aminomethylpyridine (amp) and synthesized the single-type MX chains consisting of a single aromatic in-plane ligand for the first time.

Results and Discussions

Syntheses of single-type MX chains with aromatic in-plane ligand

Rochon et al. reported the synthesis and crystal structure of $[Pt(amp)_2]Cl_2\cdot H_2O$,[10] and its single-crystalline photochromism was discovered in 2002.[11] Although its bromide analogue has never been reported, we synthesized $[Pt^{II}(amp)_2]Br_2$ (**1**) from $PtBr_2$ according to these reports. Then, $[Pt^{IV}(amp)_2Br_2]Br_2\cdot 2H_2O$ (**2**) was prepared upon addition of hydrobromic acid and hydrogen peroxide into aqueous solution of **1**. Aqueous

[a] Department of Chemistry, Graduate School of Science, Tohoku University, 6-3 Aza-Aoba, Aramaki, Aoba-ku, Sendai 980-8578, Japan.
[b] Department of Advanced Material Science, Graduate School of Frontier Sciences, The University of Tokyo, Kashiwa 277-8561, Japan.
[c] AIST-UTokyo Advanced Operando-Measurement Technology Open Innovation Laboratory, National Institute of Advanced Industrial Science and Technology, Chiba 277-8568, Japan.
[d] Advanced Institute for Materials Research, Tohoku University, 2-1-1 Katahira, Aoba-Ku, Sendai 980-8577, Japan.
[e] School of Materials Science and Engineering, Nankai University, Tianjin 300350, China.

† Footnotes relating to the title and/or authors should appear here.
Electronic Supplementary Information (ESI) available: [details of any supplementary information available should be included here]. See DOI: 10.1039/x0xx00000x

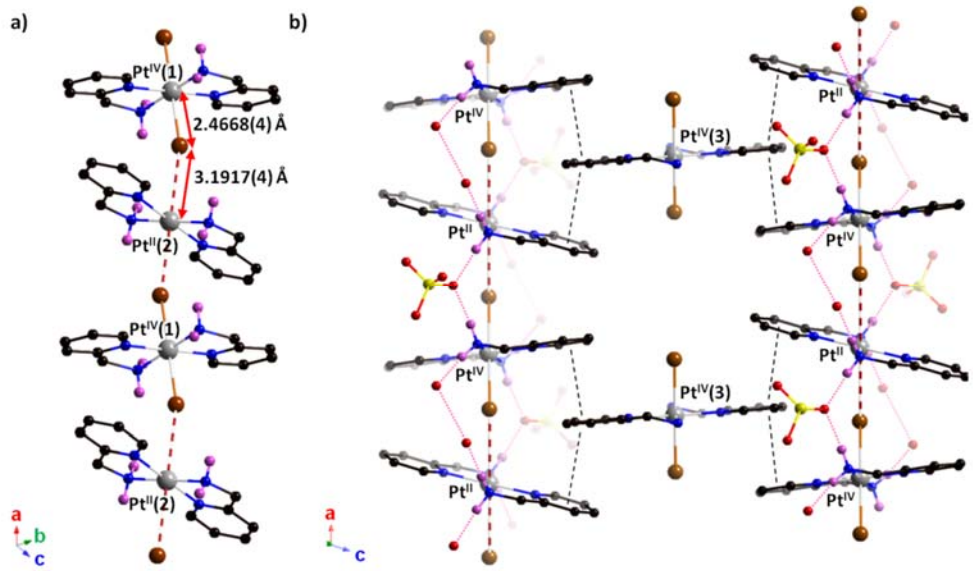

Fig. 1 a) Zigzag chain structure of **3**. Only the chain component is shown. b) Crystal structure between two adjacent MX chains in **3**. Hydrogen-bond network and π–π interactions are shown in pink dotted line and black dashed line, respectively. Counteranions and water molecules unrelated to the hydrogen-bond network along the chain are omitted for clarity. Hydrogen atoms are also omitted except those of amino groups. Light gray, Pt; brown, Br; yellow, S; black, C; blue, N; red, O; pink, H.

solution of **1** and **2** were mixed and the volume was decreased by natural evaporation. However, **1** and **2** were crystallized separately instead of the crystallization of MX chain, $[Pt(amp)_2Br]Br_2$. Thus, we tried natural evaporation with various counteranions. In presence of tetra-n-butylammonium hydrogensulfate (Bu_4NHSO_4), dark-brown plate-like crystals were obtained a day after. The formula of the crystal was determined as $[Pt^{IV}(amp)_2Br_2][Pt^{II/IV}(amp)_2Br]_2(HSO_4)_2(SO_4)_2{\cdot}13H_2O$ (**3**) by single-crystal X-ray diffraction (SCXRD) analysis and elemental analysis. The natural evaporation in presence of sodium dihydrogenphosphate (NaH_2PO_4) also afforded the single-type MX chain, $[Pt^{IV}(amp)_2Br_2][Pt^{II/IV}(amp)_2Br]_2(H_2PO_4)_6{\cdot}8H_2O$ (**4**). Although it is difficult to carry out accurate elemental analysis and bulk-scale measurements of **4** due to the crystallization with numerous by-products, the SCXRD analysis of **4** enables us to discuss its structural similarity to **3**.

Crystal structures

The crystal structure of **3** and **4** are shown in Fig. 1 and Fig. S1, respectively. The selected bond lengths and crystallographic data of **3** and **4** are shown in Tables 1 and 2, respectively. In the case of **3**, only S(1)–O(1) bond is longer (1.534(5) Å) than other S–O bonds (1.405(5)–1.471(4) Å), indicating that O(1) is protonated. Therefore, S(1) and S(2) are assigned to the sulfur atoms for HSO_4^- and SO_4^{2-}, respectively. Focusing on the structural features, SCXRD analyses of **3** and **4** delivered unique information that 1D chain co-crystallizes with Pt(IV) complex ($[Pt^{IV}(amp)_2Br_2]^{2+}$), which acts as countercation. To our knowledge, **3** and **4** are the first MX chains containing discrete Pt(IV) complex as the countercations. In the chain components, planar $[Pt(amp)_2]$ moieties are bridged by Br^- ions, which are displaced at positions away from the midpoints between two neighbouring Pt ions. The Pt(1)–Br distances are 2.4668(4) Å and 2.4860(18) Å for **3** and **4**, respectively, while Pt(2)–Br distances are 3.1917(4) Å and 3.0675(19) Å. Because a Pt^{IV}–Br distance (l_1) is usually shorter than $Pt^{II}\cdots$Br distance (l_2), Pt(1) and Pt(2) were assigned to be Pt^{IV} and Pt^{II}, respectively. Therefore, **3** and **4** are suggested to be in Pt(II/IV) mixed valence (MV) state. On the basis of ligand field theory, $4p_z$ orbitals of Br^- ions and $5d_{z^2}$ orbitals of Pt ions mainly contribute to bonding and anti-bonding orbitals, respectively. Because MV state requires partial charge transfer (CT) between Pt(IV) and Pt(II) complexes, the actual charges of each Pt ion are represented as $(4-\delta)+$ and $(2+\delta)+$, respectively, where δ indicates the degree of CT ($0 < \delta < 1$). Therefore, the bond order of Pt(IV)–Br and Pt(II)–Br bonds are "$1-\delta/2$" and "$\delta/2$", respectively. In fact, l_2 (= 3.1917(4) Å for **3** and 3.0675(19) for **4**) are shorter than the sum of van der Waals radii (3.62 Å)[12], and l_1 (= 2.4668(4) Å for **3** and 2.4860(18) Å for **4**) are slightly longer than Pt(IV)–Br length of discrete Pt(IV) countercation (2.4531(5) Å for **3** and 2.407(14) and 2.455(4)

Table 1. Selected coordination and hydrogen bond lengths, Pt^{IV}–Br distance (l_1), $Pt^{II}\cdots$Br distance (l_2) and Pt–Br–Pt distance (L) in the chain components for **3** and **4.**

	3	**4**
d(Pt–N)/Å	2.024(5)– 2.053(3)	2.007(15)–2.049(15)
d(S–O)/Å	1.405(5)–1.534(5)	
d(N···O(SO_4^{2-}))/Å	2.783(5), 2.808(6)	
d(N···OH_2)/Å	2.804(5), 2.883(7)	
d($OH_2\cdots OH_2$)/Å	2.813(6)	
d(N···O($H_2PO_4^-$))/Å		2.84(2)–3.05(3)
d(Pt^{IV}(3)–Br)/Å	2.4531(5)	2.407(14), 2.455(4)
l_1/Å	2.4668(4)	2.4860(18)
l_2/Å	3.1917(4)	3.0675(19)
L/Å	5.5939(3)	5.5258(8)

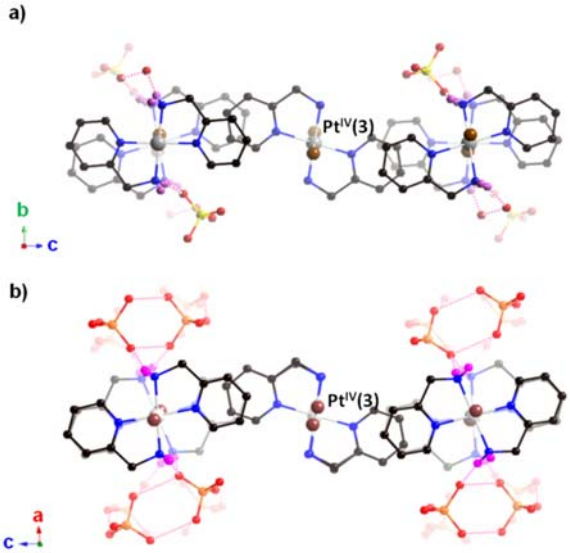

Fig. 2 Perspective view of two adjacent MX chains and intercalated Pt(IV) countercations of (a) **3** and (b) **4** projected along the chain axes. Hydrogen-bond network is shown in pink dotted line. Counteranions and water molecules unrelated to the hydrogen-bond network along the chain are omitted for clarity. Hydrogen atoms are also omitted except those of amino groups. The axial Br^- ligands of Pt(IV) countercation (containing Pt^{IV}(3) atom) in **4** are disordered in two positions. Light gray, Pt; brown, Br; yellow, S; orange, P; black, C; blue, N; red, O; pink, H.

for **4**). Moreover, CT band is observed in complex **3** as discussed later. These facts indicate that $\delta \neq 0$ and Pt^{II}···Br contact has a bonding character.

The infinite chain structure of **3** is supported by N–H····O hydrogen bonds between amino groups of amp ligands and counteranions as well as water molecules. Focusing on one side of the 1D chain, counteranions (SO_4^{2-}) and two water molecules alternately arrange to form 1D hydrogen-bond network (N–H····O(SO_4^{2-})····H–N–H····OH_2····OH_2····H–N) as shown in Fig. 1b. This arrangement is in reverse order on the opposite side of the chain. Additionally, Pt(IV) complexes provide aromatic interactions between two neighbouring chains, resulting in the formation of 2D π-stacking network. The distance between amp ligand of 1D chain and that of Pt(IV) complex is 3.4–3.5 Å, defined as face to face aryl-aryl interactions. Due to the alternate intercalation of Pt(IV) complexes into the [Pt(amp)$_2$] planer units which are bridged by Br^- ions, the units are tilted and provided the angle θ(Pt–Br–Pt) of 162.51 °. Consequently, the zigzag ···Br–Pt^{IV}–Br····Pt^{II}···· chains form along *a* axis (Fig. 1a). The disorder of bridging Br^- ions, which is common phenomenon in general PtBr chains, is not observed in **3**, probably because the two-fold periodicity of the lattice (alternate fashion of hydrogen-bond network and intercalation of Pt(IV) complexes) induces the three-dimensionally ordered MV state. The other counteranion (HSO_4^-) forms N–H····O hydrogen bond between amino groups of Pt(IV) countercation and O–H····O hydrogen bond between SO_4^{2-} ion and water molecules.

The infinite chain structure of **4** is similar to that of **3** although there are mainly two differences from **3**: (1) Only $H_2PO_4^-$ ions contribute to the 1D hydrogen-bond network of **4**

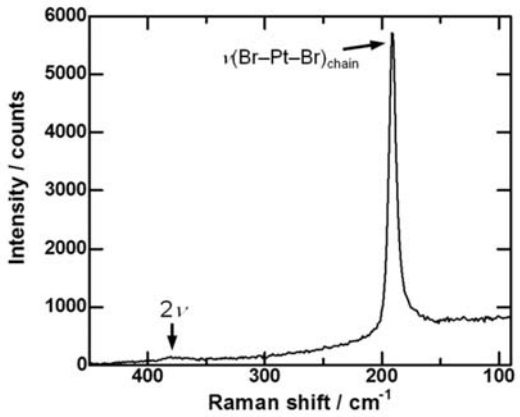

Fig. 3 Polarized Raman spectrum of **3** at room temperature measured with polarized light parallel to the chain axis (*a* axis). (λ_{ex} = 632.8 nm).

(N–H····O($H_2PO_4^-$)····H–N–H····O–H($H_2PO_4^-$)····O($H_2PO_4^-$)····H–N) as shown in Fig. S1. (2) The orientation of methylamino groups in Pt(II) and Pt(IV) components of the chain is opposite in the case of **4**, while it is nearly equal in **3**, as evidenced by the Fig. 2. Besides, the Pt(IV) countercations in **4** also form N–H····O hydrogen bond between the $H_2PO_4^-$ ions which do not contribute to the 1D hydrogen-bond network of the chain moieties mentioned above.

Polarized Raman spectra

For further investigation of the electronic states of **3**, polarized Raman spectrum was acquired. The intensities and number of Raman peaks depend on their electronic state. It is well-known that MX chains in MV state show a Raman peak attributed to X–M^{IV}–X symmetrical stretching mode ((ν(X–M^{IV}–X)).[13,14] On the other hand, those in AV state do not show any Raman signals because X–M^{III}–X symmetrical stretching mode (ν(X–M^{III}–X)) is forbidden.[7a,15] Fig. 3 shows the spectrum of single crystalline **3** measured at an excitation wavelength (λ_{ex}) of 632.8 nm (= 1.96 eV) at room temperature. The measurements were repeated with several single crystals and show good reproducibility. An intense peak at 190 cm^{-1} with weak overtone (380 cm^{-1}) was observed. These are consistent with the resonance Raman spectra of typical PtBr chains,[16] supporting that **3** forms Pt(II/IV) MV state, which is in good agreement with SCXRD analysis. Because the excitation energy (1.96 eV) is close to the charge-transfer (CT) band of **3** but is far from absorption band of Pt(IV) complex (e.g. **2**) as shown in Fig. 4, only the peak attributed to ν(Br–Pt^{IV}–Br) of the chain is enhanced. That attributed to ν(Br–Pt^{IV}–Br) of countercation ([Pt^{IV}(amp)$_2$Br$_2$]$^{2+}$), which typically appears around 212 cm^{-1},[17] is not enhanced and too weak to be observed. This resonance Raman spectrum is the characteristics of MX chains.[7a,b,13–16.]

Charge-transfer energy of 3

In order to estimate charge-transfer (CT) energy (E_{CT}), UV-Vis-NIR absorption spectra were acquired. In the present work, the spectra of amp ligand, **1** and **2** were acquired from the aqueous solution. That of **3** was obtained by the diffuse reflectance method with $BaSO_4$ followed by Kubelka-Munk

transformations. Fig. 4 shows an intense and broad band (2.46 and 4.64 eV) and weak band (around 3.5 eV) in **3**. Since amp ligand, **1** and **2** show intense absorption in the range of 4.5–5.0 eV, the band at 4.64 eV in **3** can be assigned to π-π* transition of amp ligand. Weak absorption band around 3.5 eV in **3** is almost corresponding to that around 3.7 eV in **2**, which is assigned to the Br (p_x or p_y orbitals) to Pt ($5dz^2$ orbitals)

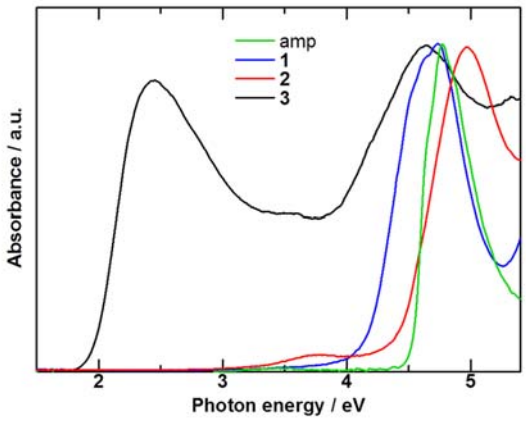

Fig. 4 UV-Vis-NIR absorption spectra of amp (green), **1** (blue) **2** (red), and **3** (black) at room temperature. The spectrum of **3** was obtained by the Kubelka-Munk transformation of diffuse reflectance spectrum measured with $BaSO_4$, and other absorption spectra were acquired from the aqueous solutions.

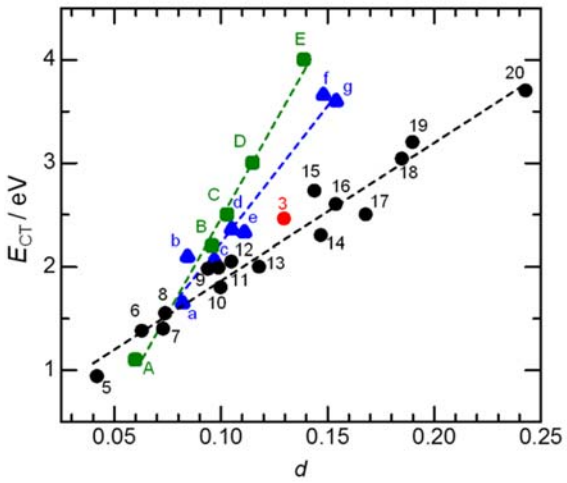

Fig. 5 CT energy (E_{CT}) of **3** and representative MX chains (M = Pt and Pd) plotted as a function of d (= $(I_2 - I_1)/L$), where I_2, I_1 and L indicate $M^{II}\cdots X$, M^{IV}–X and M–X–M distances, respectively. Color indicates the type of MX chains: black (single type), blue (ladder type), green (tube type) and red (compound **3**). The broken lines are merely to guide the eye. The data are shown for $[Pt(chxn)_2I]I_2$ (5),[22] $[Pt(en)_2I](ClO_4)_2$ (6),[2] $[Pt(chxn)_2Br]Br_4$ (7),[2] $[Pt(tn)_2Br](ClO_4)_2$ (8),[2] $[Pt(en)_2Br](ClO_4)_2$ (9),[2] $[Pt(chxn)_2Cl]Cl_2$ (10),[2] $[Pt(NH_3)_4Br](HSO_4)_2$ (11),[14] $[Pt(en)_2I](ReO_4)_2$ (12),[18] $[Pt(etn)_2Br]Br_2$ (13),[14] $[Pt(en)_2Cl](ClO_4)_2$ (14),[2] $[Pt(tn)_2Cl](BF_4)_2$ (15),[14] $[Pt(NH_3)_4Cl](HSO_4)_2$ (16),[14]$[Pt(pn)_2Cl](ClO_4)_2$ (17),[14] $[Pt(en)_2Br](ReO_4)_2$ (18),[18] $[Pt(chxn)_2Cl](ClO_4)_2$ (19),[2] $[Pt(en)_2Cl](ReO_4)_2$ (20),[18] $[\{Pt(en)I\}_2(bpym)]I_4\cdot 4H_2O$ (a),[19a] $[\{Pt(dien)Br\}_2(bpy)]Br_4\cdot 2H_2O$ (b),[8] $[\{Pt(en)Br\}_2(bpym)]Br_4\cdot 4H_2O$ (c),[19a] $[\{Pt(en)Br\}_2(bpym)]Br(ClO_4)_3\cdot H_2O$ (d),[19a] $[\{Pt(dien)Br\}_2(dach)](NO_3)_4$ (e),[19b] $[\{Pt(en)Cl\}_2(bpym)]Cl(ClO_4)_3\cdot H_2O$ (f),[19a] $[\{Pt(dien)Cl\}_2(azpy)](ClO_4)_4\cdot C_3H_6O$ (g),[19b] $[Pt(en)(bpy)I]_4(NO_3)_8\cdot 16H_2O$ (A),[9] $[Pd(chxn)]_2[Pt(chxn)(CN)_2I_2]_2(NO_3)_4$ (B),[21] $[Pt(chxn)(CN)Br]_4(NO_3)_4$ (C),[21] $[Pd(chxn)]_2[Pt(chxn)(CN)_2Br_2]_2(NO_3)_4$ (D),[21] $[Pd(chxn)]_2[Pt(chxn)(CN)_2Cl_2]_2(NO_3)_4$ (E).[21] tn = 1,3-diaminopropane, etn = ethylamine, pn = 1,2-diaminopropane, dach = trans-1,4-diaminocyclohexane, azpy = 4,4′-azopyridine, bpym = 2,2′-bipyrimidine.

transition[18] partially allowed due to the zigzag structure. The intense band at 2.46 eV, which is not observed in precursor **1** and **2**, is the characteristic feature of 1D chain. Therefore, it can be assigned to an intervalence charge transfer (IVCT) transition from the Pt^{II} $5dz^2$ orbitals to the Pt^{IV} $5dz^2$ orbitals. The E_{CT} of **3** is plotted as a function of distortion parameter d, which is defined as $(I_2 - I_1)/L$, where L indicates M–X–M distance, together with a series of MX chains (Fig. 5). It has been known that the slope of the fitted line varies among the chain system, such as single-type MX chain, two-legged ladder-type MX chains[8,19,20] and tube-type MX chains.[9,20,21] This is because the E_{CT} value theoretically depends on the dimensionality of MX-chain systems. As shown in Fig. 5, **3** seems to obey the fitted line for the single-type MX chain. This result suggests that the electronic state of **3** is scarcely perturbed by the π-conjugated ligand or the interchain interaction via π-stacking.

Significance of π-stacking

The intercalation of Pt(IV) complexes between neighbouring 1D chains indicates that π-stacking has played an important role in stabilizing the chain structure of single-type MX chains with amp ligand. Fig. 6 shows the space-filling models of the chain structure in $[Pt(chxn)_2Br]Br_2$[23] (chxn = cyclohexanediamine) and **3**. In the typical MX chains with aliphatic in-plane ligand such as chxn, little space exists between $[Pt(chxn)_2]$ moieties bridged by Br^- ions. In contrast, larger space should exist between π-conjugated plane of $[Pt(amp)_2]$ moieties. Since such a space is unfavourable for the crystal packing, unusual intercalation of Pt(IV) complex occurs to stabilize the chain structure by aromatic interaction. This work points out that either of following two requirements should be filled to develop the single-type MX-chain system with aromatic in-plane ligands: (1) Counterion contains π-conjugated plane. (2) In-plane ligand has appropriate substituent which can fill the space between aromatic in-plane

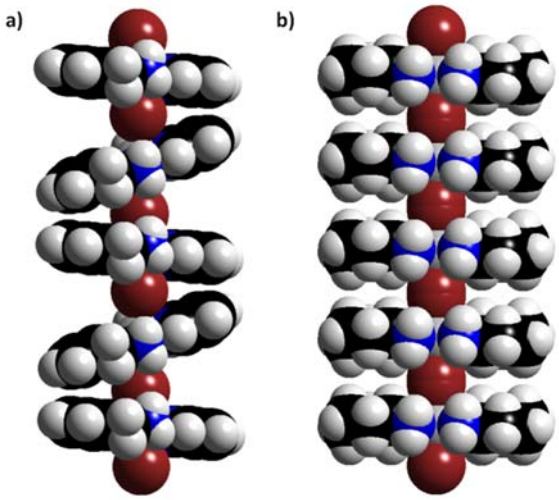

Fig. 6 Space-filling models of the chain structure of a) **3** and b) $[Pt(chxn)_2Br]Br_2$. Counterions and lattice water molecules are omitted for clarity. Light gray, Pt; brown, Br; black, C; white, H.

Table 2. Crystallographic Data for **1**, **2**, **3** and **4**.

	1	**2**	**3**	**4**
Radiation type, wave length /Å	MoKα, 0.7107	MoKα, 0.7107	MoKα, 0.7107	MoKα, 0.7107
Empirical formula	$C_{12}H_{16}Br_2N_4Pt$	$C_{12}H_{20}Br_4N_4O_2Pt$	$C_{36}H_{76}Br_4N_{12}O_{29}Pt_3S_4$	$C_{36}H_{76}Br_4N_{12}O_{32}P_6Pt_3$
Formula weight	571.20	767.05	2174.23	2279.81
Crystal system	triclinic	Monoclinic	Monoclinic	triclinic
Space group	*P*-1	*Pc*	$P2_1/c$	*P*-1
Crystal size /mm^3	0.13 × 0.11 × 0.06	0.16 × 0.14 × 0.04	0.31 × 0.11 × 0.08	0.08 × 0.04 × 0.02
a/Å	6.9135(5)	7.0635(8)	11.1877(5)	11.0044(16)
b/Å	7.2643(5)	8.3027(9)	18.4105(7)	11.0516(17)
c/Å	8.2243(6)	17.0426(18)	16.9085(7)	16.852(2)
α/°	110.7541(12)			72.019(5)
β/°	100.1651(14)	98.9090(19)	108.8236(10)	77.447(5)
γ/°	99.2081(14)			60.876(4)
V/Å^3	368.89(5)	987.42(19)	3296.4(2)	1697.4(5)
Temperature / K	298	123	298	200
Z	1	2	2	1
Density(calculated) / gcm^{-1}	2.571	2.580	2.191	2.230
Absorption coefficient /mm^{-1}	14.917	15.210	8.990	8.754
*R*1, *wR*2 [$I > 2\sigma(I)$]	0.0257, 0.02604	0.0350, 0.0565	0.0435, 0.0765	0.0754, 0.1626
*R*1, *wR*2 [all data]	0.0504, 0.0506	0.0532, 0.0608	0.0967, 0.0915	0.1392, 0.1870
F(000)	264	708	2092	1096
Goodness of fit on F^2	1.057	0.900	1.024	1.022

ligands.

Conclusions

In summary, 2-aminomethylpyridine (amp) was adopted as the aromatic in-plane ligand of quasi-1D halogen-bridged metal complexes (MX chains). $[Pt^{IV}(amp)_2Br_2][Pt^{II/IV}(amp)_2Br]_2(HSO_4)_2(SO_4)_2{\cdot}13H_2O$ (**3**) and $[Pt^{IV}(amp)_2Br_2][Pt^{II/IV}(amp)_2Br]_2(H_2PO_4)_6{\cdot}8H_2O$ (**4**) are the first single-type MX chains whose in-plane ligands consist solely of aromatic moiety. Moreover, they contain intercalated Pt(IV) complex ($[Pt^{IV}(amp)_2Br_2]^{2+}$) for the first time. These chain structures are stabilized by both aromatic interactions and hydrogen-bond networks. Single-crystal X-ray structure analysis and spectroscopic analyses confirmed that both **3** and **4** form Pt(II/IV) mixed valence (MV) state. The amp ligand can be the propitious candidate to realize multifunctional MX chains based on its rigidity and ease of functionalization via organic reactions. Our strategy and the present results open up the integrated study on MX chains and heterocyclic organic chemistry. Further studies such as the substitution effect are currently underway.

Experimental

Synthetic procedures

$PtBr_2$, 2-aminomethylpyridine were purchased from Tokyo Chemical Industry (TCI). Bu_4NHSO_4, $NaH_2PO_4{\cdot}2H_2O$, HBr (47%), H_2O_2, and acetone were purchased from Wako Chemicals. These chemicals were used without further purification.

Synthesis of $[Pt^{II}(amp)_2]Br_2$ (1): 2-aminomethylpyridine (amp) (30.3 mg, 0.28 mmol) was added to an aqueous suspension (10 mL) of $PtBr_2$ (200.0 mg, 0.564 mmol). The mixture was stirred for 10 hours at 70 °C. The clear solution was filtered and concentrated to 2 mL, then white precipitates were formed by adding acetone. The white powders were collected by a filtration and dried in air. The colourless single crystals suitable for the X-ray structural analysis were obtained by diffusion of acetone vapor (yield: 75% based on Pt). The crystal structure of **1** is shown in Fig. S3. Anal. Calc. for **1**: C 25.23, H 2.82, N 9.81. Found: C 25.38, H 3.09, N 9.75%.

Synthesis of $[Pt^{IV}(amp)_2Br_2]Br_2{\cdot}2H_2O$ (2): H_2O_2 (11.9 mg, 0.105 mmol) and conc. HBr (56.6 mg, 0.329 mmol) were added to an aqueous solution (5 mL) of $[Pt^{II}(amp)_2]Br_2$ (200.0 mg, 0.350 mmol), and then the mixture was stirred for 24 hours. The yellow solution was filtered, concentrated to 2 mL and left overnight in a refrigerator. The yellow crystals were collected by filtration and dried in air (yield: 82% based on Pt). The crystal structure of **2** is shown in Fig. S3. Anal. Calc. for **2**: C 18.80, H 2.63, N 7.30. Found: C 19.15, H 2.71, N 7.20.

Synthesis of $[Pt^{IV}(amp)_2Br_2][Pt^{II/IV}(amp)_2Br]_2(HSO_4)_2(SO_4)_2{\cdot}13H_2O$ (3): To an aqueous solution (1 mL) of $[Pt^{II}(amp)_2]Br_2$ (10.0 mg, 0.0175 mmol) and $[Pt^{IV}(amp)_2Br_2]Br_2$ (13.2 mg, 0.0172 mmol), aqueous solution (1 mL) of tetrabutylammonium hydrogensulfate (12.2 mg, 0.0359 mmol) was added, then this mixture was slowly evaporated for one day. Single crystals of **3** were obtained as red-brown plate-shaped crystals (yield: 52% based on Pt). It exhibits remarkable dichroism, i.e., strongly coloured for the light polarized along the plane direction. Anal. Calc. for **3**: C 19.89, H 3.52, N 7.73. Found: C 20.39, H 3.59, N 7.52.

Synthesis of $[Pt^{IV}(amp)_2Br_2][Pt^{II/IV}(amp)_2Br]_2(H_2PO_4)_6{\cdot}8H_2O$ (4): To an aqueous solution (1 mL) of $[Pt^{II}(amp)_2]Br_2$ (10.0 mg, 0.0175 mmol) and $[Pt^{IV}(amp)_2Br_2]Br_2$ (13.2 mg, 0.0172 mmol), aqueous solution (1 mL) of sodium dihydrogenphosphate

dihydrate ($NaH_2PO_4 \cdot 2H_2O$) (6.24 mg, 0.0400 mmol) was added, then this mixture was slowly evaporated for one day. Single crystals of **4** were obtained as grey needle-shaped crystals. It exhibits remarkable dichroism as well as **3**. Because **4** was crystallized with numerous by-products, accurate elemental analysis has not been obtained yet.

Methods

Single-crystal X-ray structural determination: Single-crystal X-ray diffraction data of **1**–**4** were collected on a Bruker APEX-II diffractometer with a APEX II CCD detector and JAPAN thermal Engineering Co., Ltd Cryo system DX-CS190LD. The crystal structures were solved by using direct methods (SIR2004[24], SHELXS-97,[25] or SHELXT[26]), followed by Fourier syntheses. Structure refinement was performed by using full matrix least-squares procedures using SHELXL[25,27] on F^2 in the Yadokari-XG2009 software.[28] CCDC-1837633, 1837634, 1837635 and 1837632 contain the supplementary crystallographic data for **1**, **2**, **3** and **4**, respectively. These data can be obtained free of charge from the Cambridge Crystallographic Data Centre.

Raman spectroscopy: Polarized Raman spectra were acquired on Renishaw Raman spectrometer with He–Ne laser (632.8 nm) and an optical microscope.

Ultraviolet-visible-near-infrared absorption spectroscopy: Ultraviolet-visible-near-infrared (UV-Vis-NIR) absorption spectra were performed with a Shimadzu UV-3100 instrument at room temperature. The absorption spectra of the free amp ligand, **1** and **2** were measured in the range of 200−1000 nm by using a quartz cuvette with a light path of 1 cm. The accuracy of the spectra was tested by repeating the measurement several times. The solid-state diffuse reflectance spectrum of **3** was obtained by using the same instrument. **3** was ground with $BaSO_4$ and loaded on to the $BaSO_4$ cake. The obtained spectrum was transformed to Kubelka-Munk function, $F(R) = (1-R)^2/2R$ (R is the diffuse reflectance of the sample as compared to $BaSO_4$), for a comparison with other spectra.

Elemental Analysis: Elemental analyses were performed at the Research and Analytical Centre for Giant Molecules, Tohoku University.

Conflicts of interest

The authors declare no competing financial interests.

Acknowledgements

This work was partly supported by JSPS KAKENHI Grant Numbers JP15K17828 (H.I.), JP18K14233 (H.I.), JP18H04498 (H.I.), JP18H01166 (H.O.) and JP26248015 (M.Y.), by the Sumitomo Foundation (H.I.), by the CASIO Science Promotion Foundation (H.I.), by the Ogasawara Foundation for the Promotion of Science and Engineering (H.I.), by the Program for Interdisciplinary Research in Tohoku University Frontier Research Institute for Interdisciplinary Sciences (H.I.), and CREST, JST Grant Numbers JPMJCR1661 (H.O.) and JPMJCR12L3 (M.Y. and H.I.). M.Y. thanks the support by the 111 project (B18030) from China. Preliminary crystal structure analysis was performed under the approval of the Photon Factory Program Advisory Committee (Proposal No. 2016G040 and 2018G083, beamline NW2A).

Notes and references

1(a) J. S. Miller, Extended Linear Chain Compounds, Plenum Press, New York, 1982; (b) M. Yamashita and H. Okamoto, Material Designs and New Physical Properties in MX- and MMX-Chain Compounds, Springer, Wien, 2013; (c) G. Givaja, P. Amo-Ochoa, C. J. Gómez-García and F. Zamora, *Chem. Soc. Rev.*, 2012, **41**, 115; (d) H. Iguchi, S. Takaishi and M. Yamashita, *Chem. Lett.*, 2014, **43**, 69.

2 H. Okamoto and M. Yamashita, *Bull. Chem. Soc. Jpn.,* 1998, **71**, 2023.

3 (a) Y. Iwasa, E. Funatsu, T. Hasegawa, T. Koda and M. Yamashita, *Appl. Phys. Lett.,* 1991, **59**, 2219. (b) H. Kishida, H. Matsuzaki, H. Okamoto, T. Manabe, M. Yamashita, Y. Taguchi and Y. Tokura, *Nature,* 2000, **405**, 929.

4 S. Iwai and H. Okamoto, *Phys. Soc. Jpn.,* 2006, **75**, 011007.

5 S. Takaishi, Y. Tobu, H. Kitagawa, A. Goto, T. Shimizu, T. Okubo, T. Mitani and R. Ikeda, *J. Am. Chem. Soc.,* 2004, **126**, 1614.

6 M. R. Mian, H. Iguchi, S. Takaishi, H. Murasugi, T. Miyamoto, H. Okamoto, H. Tanaka, S. Kuroda, B. K. Breedlove and M. Yamashita, *J. Am. Chem. Soc.,* 2017, **139**, 6562.

7 (a) S. Takaishi, M. Takamura, T. Kajiwara, H. Miyasaka, M. Yamashita, M. Iwata, H. Matsuzaki, H. Okamoto, H. Tanaka, S. Kuroda, H. Nishikawa, H. Oshio, K. Kato and M. Takata, *J. Am. Chem. Soc*., 2008, **130**, 12080; (b) S. Kumagai, S. Takaishi, B. K. Breedlove, H. Okamoto, H. Tanaka, S. Kuroda and M. Yamashita, *Chem. Commun.,* 2014, **50**, 8382; (c) S. Kumagai, S. Takaishi, H. Iguchi, B. K. Breedlove, T. Kaneko, H. Ito, S. Kuroda and M. Yamashita, *Inorg. Chem.,* 2018, **57**, 12.

8 A. Kobayashi and H. Kitagawa, *J. Am. Chem. Soc.,* 2006, **128**, 12066.

9 K. Otsubo, Y. Wakabayashi, J. Ohara, S. Yamamoto, H. Matsuzaki, H. Okamoto and H. Kitagawa, *Nat. Mater.,* 2011, **10**, 291.

10 F. D. Rochon and R. Melanson, *Acta Crystallogr.,* 1979, **B35**, 2313.

11 H. Nishimura and N. Matsushita, *Chem. Lett.,* 2002, **31**, 930.

12 A. Bondi, *J. Phys. Chem*., 1964, **68**, 441.

13 (a) R. J. H. Clark, M. Kurmoo, H. J. Keller, B. Keppler and U. Traeger, *J. Chem. Soc., Dalton Trans.,* 1980, 2498; (b) R. J. H. Clark, M. Kurmoo, D. N. Mountney and H. Toftlund, *J. Chem. Soc., Dalton Trans.,* 1982, 1851; (c) H. Tanino and K. Kobayashi, *J. Phys. Soc. Jpn.,* 1983, **52**, 1446. (d) M. R. Mian, H. Iguchi, M. Miyata, S. Takaishi, H. Yamakawa, T. Terashige, T. Miyamoto, H. Okamoto and M. Yamashita, *Z. Anorg. Allg. Chem*., 2018, **644**, 646.

14 R. J. H. Clark, in *Advances in Infrared and Raman Spectroscopy Volume 11*, ed. R. J. H. Clark and R. E. Hester, Wiley, Hayden, 1984, p. 95.

15 (a) T. Yoshida, S. Takaishi, H. Iguchi, H. Okamoto, H. Tanaka, S. Kuroda, Y. Hosomi, S. Yoshida, H. Shigekawa, T. Kojima, H. Ohtsu, M. Kawano, B. K. Breedlove, L. Guerin and M. Yamashita, *ChemistrySelect*, 2016, **1**, 259.

16 (a) S. Kumagai, H. Iguchi, S. Takaishi, B. K. Breedlove, M. Yamashita, H. Matsuzaki, H. Okamoto, K. Kato and M. Takata, *Inorg. Chem.,* 2014, **53**, 11764. (b) M. R. Mian, H. Iguchi, S. Takaishi, U. Afrin, T. Miyamoto, H. Okamoto, and M. Yamashita, *Inorg. Chem.,* 2019, **58**, 114.

17 C. G. Barraclough, R. J. H. Clark, M. Kurmoo, *J. Mol. Struct*., 1982, **79**, 239.

18 S. Kumagai, S. Takaishi, M. Gao, H. Iguchi, B. K. Breedlove and M. Yamashita, *Inorg. Chem.,* 2018, **57**, 3775.

19 (a) D. Kawakami, M. Yamashita, S. Matsunaga, S. Takaishi, T. Kajiwara, H. Miyasaka, K. Sugiura, H. Matsuzaki, H. Okamoto, Y. Wakabayashi and H. Sawa, *Angew. Chem., Int. Ed.,* 2006, **45**, 7214. (b) K. Otsubo, A. Kobayashi, K. Sugimoto, A. Fujiwara and H. Kitagawa, *Inorg. Chem.,* 2014, **53**, 1229.
20 K. Otsubo and H. Kitagawa, *CrystEngComm.,* 2014, **16**, 6277.
21 K. Otake, K. Otsubo, K. Sugimoto, A. Fujiwara and H. Kitagawa, *Angew. Chem., Int. Ed.,* 2016, **55**, 6448.
22 S. Takaishi, D. Kawakami, M. Yamashita, M. Sasaki, T. Kajiwara, H. Miyasaka, K. Sugiura, Y. Wakabayashi, H. Sawa, H. Matsuzaki, H. Kishida, H. Okamoto, H. Watanabe, H Tanaka, K. Marumoto, H. Ito and S. Kuroda, *J. Am. Chem. Soc.,* 2006, **128**, 6420.
23 B. Scott, S. P. Love, G. S. Kanner, S. R. Johnson, M. P. Wilkerson, M. Berkey, B. I. Swanson, A. Saxena, X.Z. Huang and A. R. Bishop, *J. Mol. Struct.,* 1995, **356**, 207.
24 M. C. Burla, R. Caliandro, M. Camalli, B. Carrozzini, G. L. Cascarano, L. De Caro, C. Giacovazzo, G. Polidoria and R. Spagnac, *J. Appl. Cryst.,* 2005, **38**, 381.
25 G. M. Sheldrick, *Acta Crystallogr.,* 2008, **A64**, 112.
26 G. M. Sheldrick, *Acta Crystallogr.,* 2015, **A71**, 3.
27 G. M. Sheldrick, *Acta Crystallogr.,* 2015, **C71**, 3.
28 K. Wakita, Yadokari-XG, Software for Crystal Structure Analyses, 2001; Release of Software (Yadokari-XG 2009) for Crystal Structure Analyses, C. Kabuto, S. Akine, T. Nemoto, E. Kwon, *J. Crystallogr. Soc. Jpn.,* 2009, **51**, 218.